Physica B 404 (2009) 1398–1403

Contents lists available at ScienceDirect

Physica B

journal homepage: www.elsevier.com/locate/physb

Pulsed injection metal organic chemical vapour deposition and characterisation of thin CaO films

R.P. Borges [a,*], P. Ferreira [b], A. Saraiva [a], R. Gonçalves [a,1], M.A. Rosa [a], A.P. Gonçalves [a,c], R.C. da Silva [d,e], S. Magalhães [d], M.J.V. Lourenço [f,g], F.J.V. Santos [f,g], M. Godinho [a,h]

[a] Centro de Física da Matéria Condensada, Universidade de Lisboa, Campo Grande, Ed. C8, 1749-016 Lisboa, Portugal
[b] Departamento de Engenharia Cerâmica e do Vidro, CICECO, Universidade de Aveiro, Campus Universitário de Santiago, 3810-193 Aveiro, Portugal
[c] Departamento de Química, Instituto Tecnológico e Nuclear, P-2686-953 Sacavém, Portugal
[d] Laboratório de Feixe de Iões, Dep. Física, Instituto Tecnológico e Nuclear, Estrada Nacional 10, 2686-953 Sacavém, Portugal
[e] Centro de Física Nuclear da Universidade de Lisboa, Av. Prof. Gama Pinto 2, 1649-003 Lisboa, Portugal
[f] Centro de Ciências Moleculares e Materiais, Faculdade de Ciências da Universidade de Lisboa, Campo Grande, Ed. C8, 1749-016, Lisboa, Portugal
[g] Departamento de Química e Bioquímica, Faculdade de Ciências da Universidade de Lisboa, Campo Grande, Ed. C8, 1749-016 Lisboa, Portugal
[h] Dep. de Física, Faculdade de Ciências, Universidade de Lisboa, Campo Grande, Ed. C8, 1749-016 Lisboa, Portugal

ARTICLE INFO

Article history:
Received 29 July 2008
Received in revised form
2 December 2008
Accepted 22 December 2008

Keywords:
CaO
Pulsed injection MOCVD
RBS

ABSTRACT

Thin films of CaO were grown on silicon (Si) and lanthanum aluminate ($LaAlO_3$) substrates by pulsed injection metal-organic chemical vapour deposition in a vertical injection MOCVD system. Growth parameters were systematically varied to study their effect on film growth and quality and to determine the optimal growth conditions for this material. Film quality and growth rate were evaluated by atomic force microscopy, X-ray diffraction and Rutherford Backscattering Spectroscopy measurements. Optimised conditions allowed growing transparent, single phase films textured along the (0 0 l) direction.

1. Introduction

Oxide materials have been one of the most attractive research topics in physics and materials science for the last two decades. Materials such as Fe_3O_4, CrO_2, manganese perovskites, double and layered perovskites, $BiFeO_3$ and more recently transition metal doped semiconductors such as ZnO and TiO_2 have revealed new and exciting phenomena and challenged our views on solid state physics.

Calcium oxide (CaO) has a wide range of applications in the field of materials research. Pure CaO has a rock salt structure with a lattice parameter $a = 0.481059$ nm (JCPDS File No 4-777), and may be found as a transparent crystalline solid or white amorphous material. It has a wide band-gap of 7 eV, making it very useful for applications where electrical isolation is required, such as cooling blankets for nuclear reactors [1]. This oxide is often investigated as a component in catalytic powder materials [2] or cements [3] and can also be used as dopant to modify electrical and optical properties of materials like ZrO_2 [4] and HfO_2 [5] or to stabilise materials as cubic zirconia [6]. Band structure calculations have shown that Ca vacancies in CaO could have an associated magnetic moment making this material attractive as a magnetic semiconductor [7]. The CaO crystalline structure is compatible with perovskite type structures, as in the case of the so-called Ruddlesden–Popper oxide phases where perovskite layers alternate with a layer of CaO [8]. The fabrication of perovskites/CaO multilayers may provide an artificial route to produce the magnetoresistive Ruddlesden–Popper phases. The growth of more than one layer of CaO could allow incorporating a barrier in an all oxide magnetic tunnel junction.

There are few reports on the deposition of CaO films. Kambe and co-workers used a two stage process by first depositing $Ca(OH)_2$ on MgO using pulsed laser deposition and radio frequency sputtering. The calcium hydroxide films were then heat treated to obtain CaO [9]. Polycrystalline CaO films were deposited on MgO using a chemical solution deposition method [10], while epitaxial films have been deposited on MgO by radio frequency plasma-assisted MBE [11]. In the present work CaO thin films were grown using a Pulsed Injection Metal Organic Chemical Vapour Deposition (PI-MOCVD) reactor. In this technique a room temperature solution of the precursor in an organic solvent is injected in the form of small droplets inside the reactor where

* Corresponding author.
E-mail addresses: rpborges@fc.ul.pt (R.P. Borges), rjbarrosog@hotmail.com (R. Gonçalves).
[1] Present adress: Atlantic Pharma, R. Tapada Grande no. 2, Abrunheira, 2710-089 Sintra, Portugal.

0921-4526/$ - see front matter © 2009 Elsevier B.V. All rights reserved.
doi:10.1016/j.physb.2008.12.031

flash vapourisation occurs followed by transport of the reactive species to the deposition site. The system has great flexibility allowing the study of subtle variations in stoichiometry, or the stacking of different compounds at nanometric scale. The main difference between this technique and classical MOCVD sources using bubblers or sublimators is that the flow rate of the active species is not fixed by the source temperature and the vector gas flow, but only by the feeding rate of the precursor inside the evaporator [12]. PI-MOCVD has been used to deposit a wide variety of oxides like $YBa_2Cu_3O_7$ [13], $La_{1-x}(Sr,Ca)_xMnO_3$ and $La_{1-x}Sr_xFe_{1-y}Co_yO_3$ [14], Co_3O_4 [15] or $Zn_{1-x}Co_xO$ [16].

In the present work, the variation of deposition conditions for CaO was carried out within a range compatible with the usual conditions used to deposit manganese perovskites and other oxides. The use of CaO in multilayers, tunnel junctions or the artificial production of Ruddlesden–Popper phases can be made possible by establishing a set of common thermodynamic conditions for the deposition of the different materials.

2. Experimental details

CaO thin films were grown on (0 0 1) oriented silicon (Si) and $LaAlO_3$ (LAO) substrates by a PI-MOCVD technique. The $Ca(tmhd)_2$ (tmhd = 2,2,6,6-tetramethyl-3,5-heptadionate) precursor was prepared as reported in the literature [17]. The films were grown from a solution of $Ca(tmhd)_2$ in monoglyme ($C_4H_{10}O_2$), with concentrations varying between 0.012 M and 0.050 M and substrate temperatures in the range 650–850 °C. All films were deposited under a pressure of 667 Pa with oxygen partial pressure of 267 Pa. Ar was used as a carrier gas with a flow rate of 900 ml/min. The number of droplets injected in the reactor was varied between 50 and 1800, having an average mass of 1.59 mg with a relative deviation of 9%. The solution injector valve was operated with an opening frequency of 2 Hz and an opening time of 2 ms. After each deposition the films were slowly cooled down to room temperature under 1 bar of O_2. Three series of films were grown by varying one of the following parameters: substrate temperature, solution concentration and number of injected droplets.

The crystalline structure of the films was determined using X-ray diffraction (XRD) in a θ–2θ geometry with Cu K_α radiation of 1.540598 Å wavelength. Surface morphology was studied by atomic force microscopy (AFM) in AC mode. Rutherford Backscattering Spectroscopy (RBS) was also used to determine the thickness and composition of the films.

3. Results and discussion

Before attempting the deposition of CaO films, the thermal stability and volatility of the precursor $Ca(tmhd)_2$ were evaluated by thermogravimetric (TG) analysis and differential scanning calorimetry (DSC) carried out in a nitrogen flow under atmospheric pressure. A Setaram TG-DSC111, temperature calibrated with LGC standard reference materials (Hg, In, Sn, Pb), energy calibrated by Joule effect and checked with a standard reference material (Sapphire NIST SRM 720) was used. Samples of the precursor ($\approx$10 mg) were weighed into aluminum crucibles, and the DSC scans were performed at a 5 °C/min rate, from room temperature to 350 °C. The stability of the samples and accuracy of the determinations were ensured performing 3 different runs showing no thermal hysteresis and giving reproducible results. Fig. 1 presents one of these TG-DSC runs. The TG curve shows two main mass losses in the ranges 130–220 °C (mass loss 5.7%) and 220–350 °C (total residue 31%, including a 600 s delay at 350 °C not shown on Fig. 1).

Mass spectrometric (MS) experiments were also carried out on a Thermoquest LCQ Duo quadrupole ion trap mass spectrometer in order to ascertain characteristic patterns based on 10–100 scans [18]. MS data is consistent with the presence of the following compounds in the gas phase: $Ca_2(tmhd)_4$, $Ca_2(tmhd)_3$, $Ca(tmhd)_3$, $Ca_2(tmhd)_2$ and $Ca(tmhd)_2$, molecular peaks from other substances not been detectable. The fragmentation spectra of these molecular peaks are also consistent with the expected and known cleavages for this compound [19].

For optimum film deposition, the decomposition of the precursor should only occur in the volume surrounding the substrate and consequently an appropriate evaporator temperature has to be chosen in order to avoid early decomposition. The TG-DSC runs show that significant chemical changes of the precursor occur only for temperatures higher than 220 °C. From these results an evaporator temperature of 200 °C was chosen for all depositions.

The films were deposited on LAO substrates due to its perovskite structure, similar to that of the manganese Ruddlesden–Popper phases. Simultaneous depositions were also made on Si substrates and these samples were used for RBS measurements, as described below. LAO has a distorted perovskite structure with $a = 0.3788$ nm [20] and Si crystallises in a diamond structure with a lattice parameter $a = 0.5431$ nm [21], while bulk CaO has a lattice parameter of 0.4811 nm. Considering the lattice parameters of the different structures one can expect that the

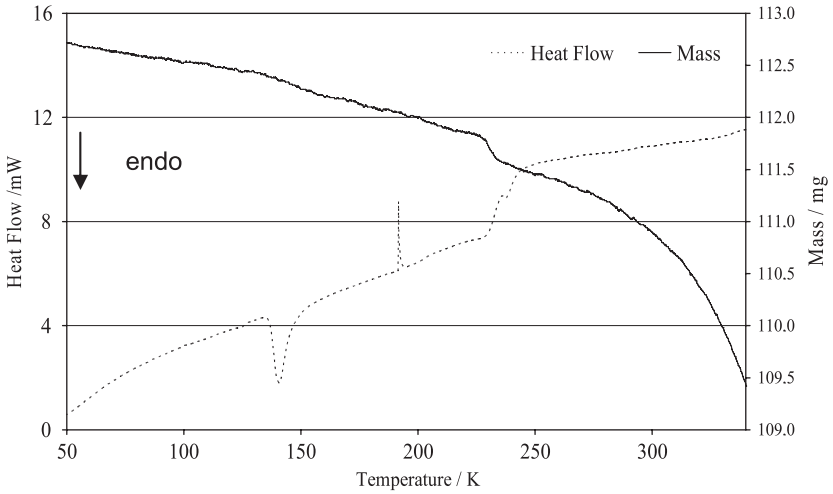

Fig. 1. TG-DSC curve of $Ca(tmhd)_2$ in a pure nitrogen atmosphere. (endo = endothermic). The mass scale represented in the graph refers to the total mass crucible+sample.

substrate can somehow condition the growth mode of the films, as the lattice mismatch, defined as

$$\frac{a_{film} - a_{substrate}}{a_{substrate}}$$

is an important factor in the setting of crystal orientation. For LAO and Si substrates the lattice mismatch with bulk CaO should be of 27.0% and −11.4%, respectively. In the case of CaO films deposited on LAO the mismatch is very large and either the films grow from an initially amorphous layer or there is an alternative orientation to accommodate the two lattices. For a growth of CaO with the edge of its cubic cell parallel to the face diagonal of LAO ($\sqrt{2}a = 0.5357$ nm) the lattice mismatch should be reduced to −10.2%. The growth with this alternative orientation is confirmed by the ϕ-scans (Fig. 2) obtained for the case of CaO deposited on LAO substrates. In order to evaluate the crystal quality of the Si and LAO substrates an asymmetrical rocking curve around the (2 2 0) reflection was performed. The detector was placed at 47.30° and 114.59°, respectively, and Ψ was null as it is the standard procedure for asymmetrical reflections. Nevertheless, the Ψ scan for the Si (2 2 0) reflection optimisation didn't provide any significant changes. When the exact Bragg conditions were fulfilled for each substrate, the sample was rotated around its normal surface axis in order to obtain the so-called ϕ-scans. The same procedure was done for the CaO layers. It was observed that the (2 2 0) plane of CaO is aligned with the same direction in the case of the Si substrate but is rotated by 45° for the films deposited on LAO. One should note that this is an in-plane rotation and CaO grows with the c-axis perpendicular to the substrate surface. Due to this preferred orientation in the case of LAO the lattice mismatch becomes very similar for deposition on both substrates. One can expect very similar tensile strains and growth modes in both cases.

To evaluate the effect of substrate temperature on film growth a series of films was grown using a solution concentration of 0.03 M and an evaporator temperature of 200 °C. Each film was formed by injecting 1200 droplets and the substrate temperature was varied between 600 °C and 850 °C. In Fig. 3a the growth rate as a function of temperature is shown for this series of films. As the substrate temperature increases from 600 to 650 °C the deposition rate grows suggesting a kinetically limited growth. Growth rate is maximum in the temperature region 650–700 °C (diffusion controlled growth) and decreases for higher temperatures probably due to desorption or decomposition of the precursor at higher temperatures, similar to the behaviour observed for the deposition of other oxides using a similar technique [22]. Fig. 3b shows the XRD patterns for each temperature studied. For deposition temperatures below 700 °C only the (0 0 2) peak of CaO is observed, whereas for substrate temperatures of 700 and 725 °C it is possible to detect the (0 0 2) and (0 0 4) reflections of CaO. For the highest substrate temperature of 850 °C the intensity of the CaO peaks is greatly reduced. The CaO lattice parameter calculated from the (0 0 2) peak is on

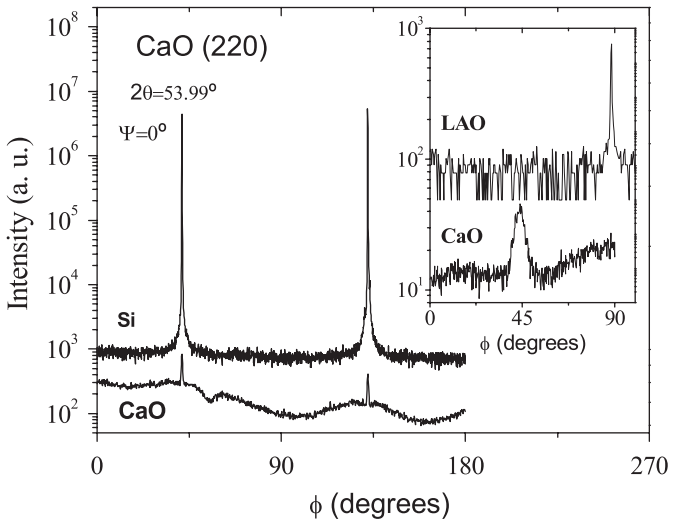

Fig. 2. Φ-scans around the (2 2 0) Si/CaO asymmetrical reflections. The CaO film adopts the Si symmetry in in-plane and out-of-plane directions. The inset shows the ϕ-scan for a film deposited on LAO and the rotation of 45° between film and substrate. The (2 2 0) reflection is located at 47.30° and 114.59° for Si and LAO, respectively.

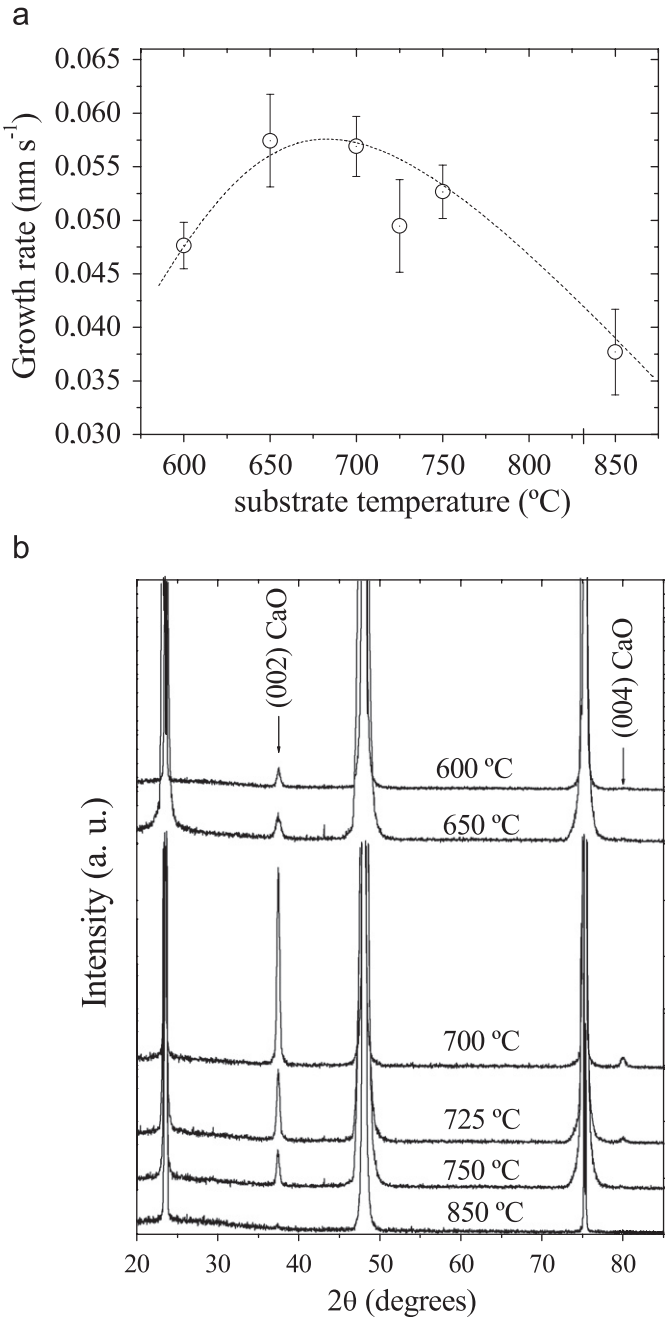

Fig. 3. (a) Deposition rate of CaO as a function of substrate temperature. The dashed line is only a guide to the eye and (b) X-ray diffraction patterns of CaO thin films as a function of substrate temperature.

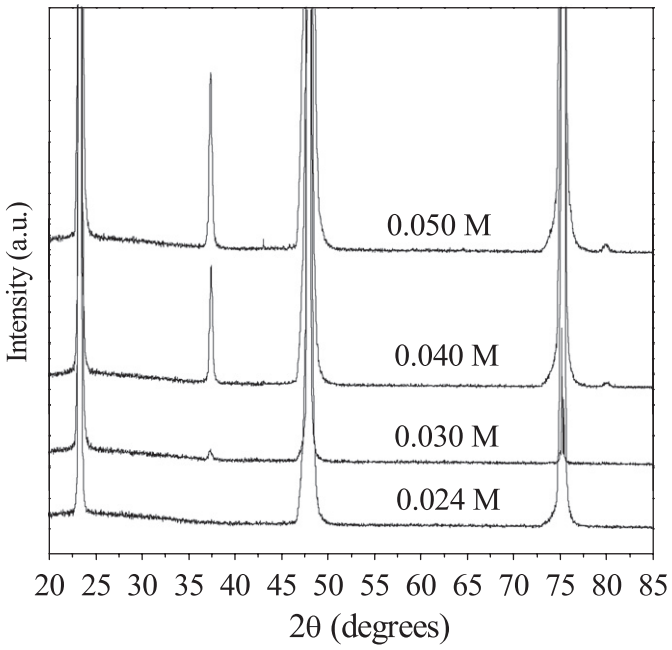

Fig. 4. X-ray diffraction pattern of CaO films deposited from solutions of different concentrations of precursor.

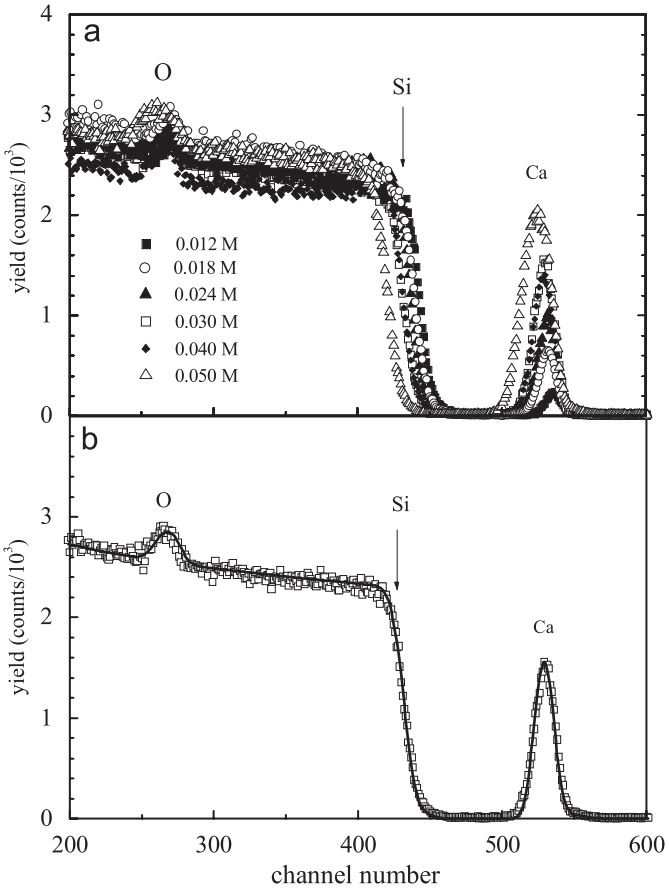

Fig. 5. (a) RBS spectra for the series of films deposited from solutions of different concentrations of precursor and (b) a fit of the spectrum obtained for the film resulting from a solution concentration of 0.03 M.

average 0.18% smaller than the bulk value, in agreement with the expected effect of tensile strain mentioned above, and shows no significant variation with temperature changes within the values tested. The grain size, estimated using Scherrer's formula

$$D = \frac{k\lambda}{B\cos\theta}$$

where D is the dimension of the crystallites, k is 0.9 and B is the full width at half maximum of the diffraction peak under analysis, has a maximum value of 19.6 nm for the film deposited at 750 °C. The roughness of the films, determined by using the program Gwyddion on AFM topographic images, has an average value of 22 nm and does not show any particular trend with the change in substrate temperature. The film deposited at 700 °C combines a higher deposition rate with the most intense (0 0 2) diffraction peak and a large grain size (19 nm) suggesting the best crystalline properties. This temperature was used consequently for the deposition of all other samples.

The effect of the solution concentration was assessed through the deposition of a series of films for which the evaporator and substrate temperatures were kept constant at 200 and 700 °C, respectively, and by using 1800 droplets of precursor solution to form each film. The solution concentration values were varied within the range 0.012–0.05 M. The X-ray analysis of this series of films (Fig. 4) shows that for concentrations below 0.03 M there is no signature of CaO deposition and only the LAO substrate peaks are visible. For a precursor solution of 0.03 M the (0 0 2) diffraction peak of CaO appears around $2\theta = 37.4°$; for higher concentration values the intensity of this peak increases and another peak appears around $2\theta = 79.9°$ corresponding to the (0 0 4) planes of CaO. The lattice parameter of the films, which does not seem to be affected by the solution concentration, is on average 0.14% smaller than that of the bulk material, again in agreement with the tensile strain expected for these films. The calculated dimensions of the CaO crystallites, obtained by applying Scherrer's formula to the (0 0 2) peak is in the range 19–25 nm. There is an increase of film roughness with increasing precursor solution concentration.

From RBS analysis the presence of CaO is confirmed for all samples. As the RBS edge for LAO overlaps that of Ca, making the analysis more difficult, all RBS results were obtained for films deposited on Si substrates, as in this case the edges for Si and Ca are well separated (Fig. 5). RBS spectra show that for some films there is contamination from the silver paste used to glue the substrates inside the deposition chamber. This contamination is of the order of 1 at% and, apart from the RBS signal, it does not seem to influence the film properties. The fits of the RBS spectra show that for the films deposited with the three lower concentrations (0.012, 0.018 and 0.024 M), Si is detected at the surface layers. This indicates a low degree of coverage of the substrate resulting in the formation of a discontinuous deposit through an island-growth mode. For the number of solution droplets used in this series (1800), our RBS results allow concluding that only concentrations equal to or higher than 0.03 M provide full coverage of the substrate, as inferred by the absence of the Si signal from the surface layers. These results are consistent with the XRD data that show no CaO diffraction peaks for concentration values below 0.030 M, indicating that the deposition of CaO is not homogeneous in the case of low precursor concentrations and that the crystallites are either amorphous or too small to produce a detectable diffraction pattern.

With the deposition conditions determined from the two previous series, and using a solution concentration of 0.03 M, five films were deposited changing the number of injected droplets between 50 and 1000.

The diffraction patterns of these films are presented in Fig. 6. The data show that the films resulting from the injection of 50 and

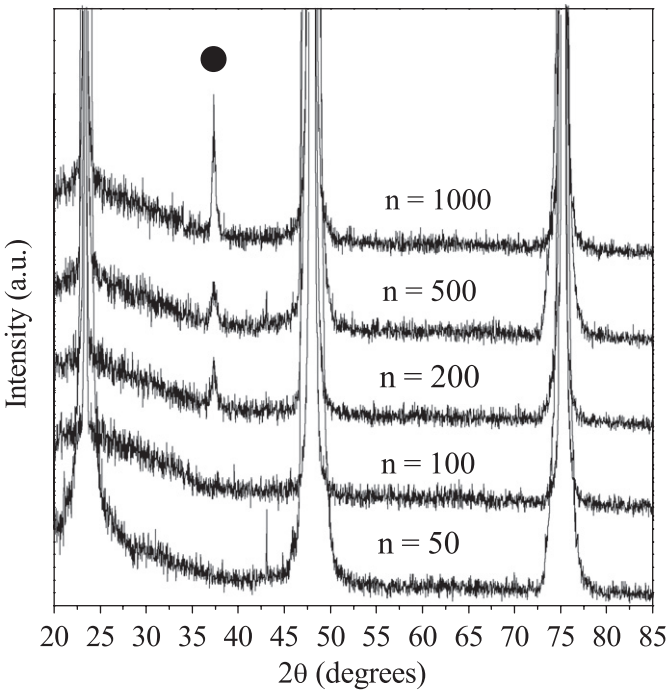

Fig. 6. X-ray diffraction pattern of CaO films as a function of film thickness.

100 droplets do not present any CaO diffraction peaks and that for the remaining samples, the intensity of the observed CaO peak increases with the number of injected droplets. The lattice parameter *c* has an average value of 0.4808 nm that does not change significantly from 200 to 1000 injected droplets. Once again this value, which is smaller than the CaO bulk lattice parameter, is explained by the tensile strain induced by the substrate.

The thickness of this series of films determined from the RBS analysis is shown in Fig. 7(a). The data show a linear variation of thickness with the number of injected droplets giving a growth rate of 0.020 nm/droplet. The obtained growth rate is lower but of the same order of magnitude as that obtained for $SrTiO_3$ layers (0.042 nm/droplet) deposited using the same technique [23]. RBS analysis also shows that only the films deposited with 1000 or more droplets are continuous, the full coverage of the substrate being achieved at some number between 500 and 1000 droplets. Because of the discontinuities in substrate coverage the determined growth rate is only indicative of average film thickness.

AFM measurements confirm the previous results in both topographic and phase imaging analysing modes. Phase imaging is sensitive to material properties such as chemical composition, stiffness and adhesion [24], and a variation of such properties gives rise to contrasts in the AFM phase maps. Figs. 8(a) and (c) show the topography of the deposits on LAO substrates resulting from the injection of 50 and 1000 droplets, respectively. In Fig. 8(b) the phase image of the film deposited with 50 droplets shows a clear contrast between a number of CaO crystallites and the background of the LAO substrate. This contrast is absent in the sample deposited with 1000 droplets, as shown in Fig. 8(d). As both samples have very similar values of surface roughness, the contrast in Fig. 8(b) is not originated by the topographic features. These results confirm a dominant island growth mode for the deposition of CaO as already observed for the films obtained with different solution concentrations. There is also good agreement between the AFM and RBS results regarding the degree of coverage of the substrates.

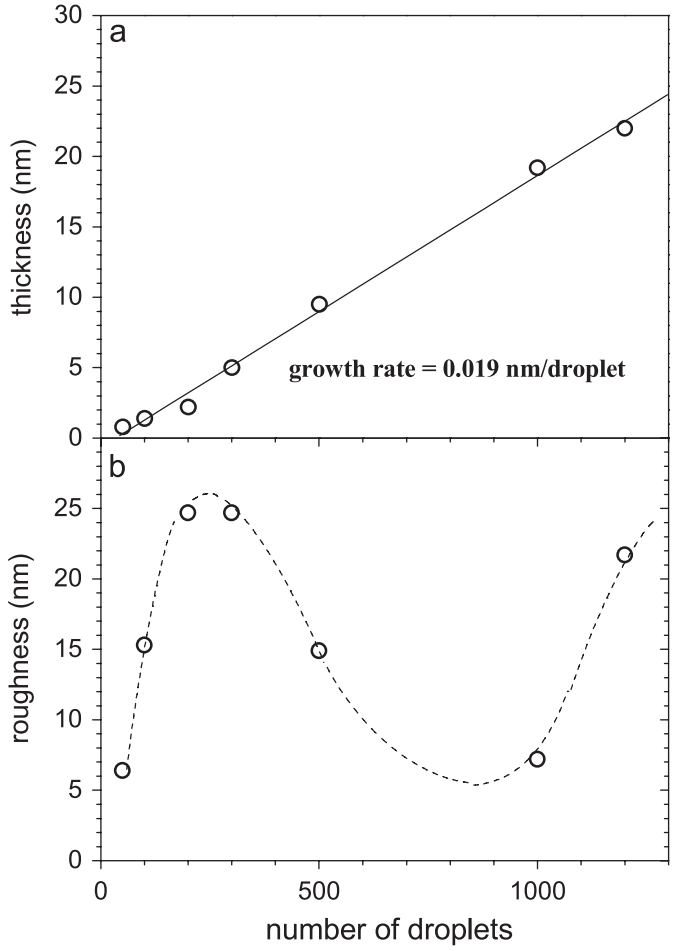

Fig. 7. (a) Average film thickness determined by RBS as a function of the number of injected droplets and (b) surface roughness determined by AFM of CaO films as a function of the number of injected droplets.

The variation of the film surface roughness with the number of droplets determined by analysis of the AFM images is depicted in Fig. 7(b), where the values corresponding to the film deposited at 700 °C in the temperature series (1200 droplets) has been added. The results show that there is a strong initial increase of surface roughness with increase of the number of injected droplets up to a value of ~25 nm corresponding to a film formed by 200 droplets. For higher number of droplets the roughness of the films decreases to a minimum value of ~7 nm for 1000 droplets and then increases again to a maximum of 22 nm for the film with 1200 droplets. We attribute this behaviour of the surface roughness to the formation of new aggregates on top of the continuous layer after the coalescence of the islands. This suggests a switch of growth mode from island (or Volmer–Weber) mode to a Stranski–Krastanov mode once a continuous layer is formed.

4. Conclusions

The deposition conditions of CaO by pulsed injection MOCVD have been determined. The films are formed by an island growth mode giving rise to transparent single phase films textured along the (0 0 1) direction. The in-plane orientation of the films is different for the two substrates used (Si and LAO) but in both cases an induced tensile strain leads to *c* lattice parameter values smaller than the bulk values. The films are initially formed through an island growth mode and become continuous for

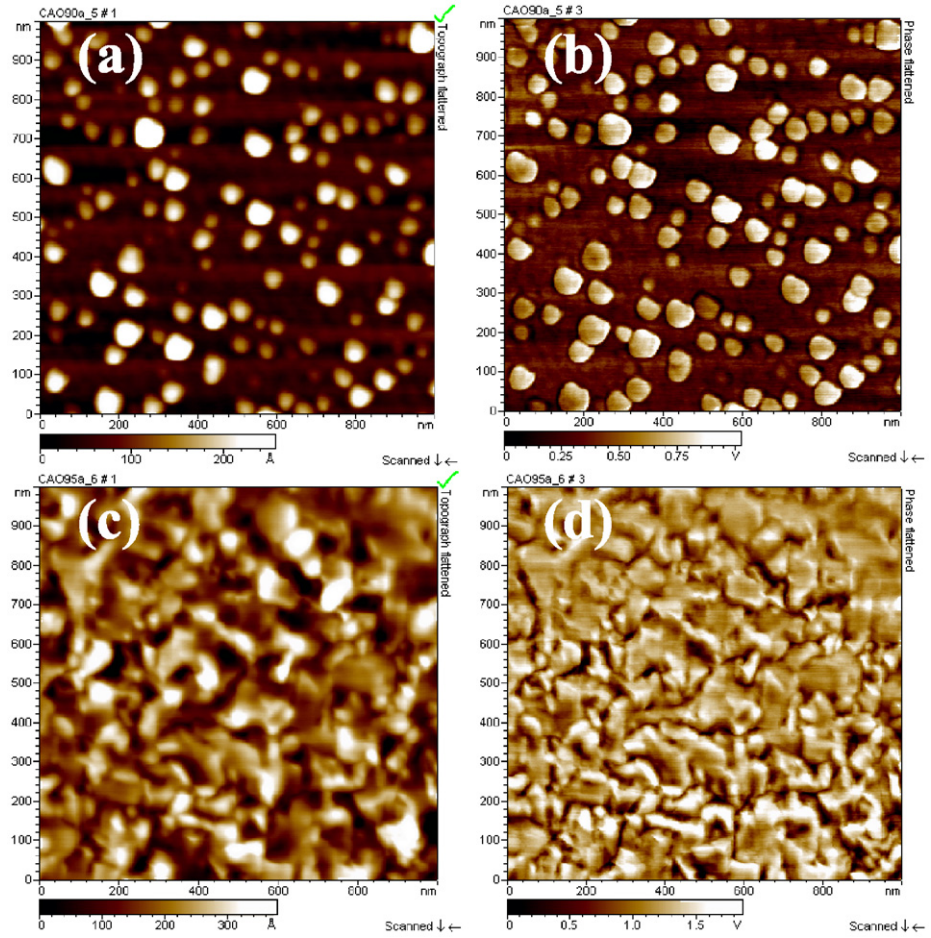

Fig. 8. (a) and (c) AFM topographic images of films deposited by injection of 50 and 1000 droplets, respectively, (b) and (d) Show the phase imaging of the same areas scanned in (a) and (d).

thicknesses between 10 and 20 nm. New aggregates seem to be formed after coalescence of the islands leading to an increase of the surface roughness.

Acknowledgements

This work was financed by the Portuguese Foundation for Science and Technology (FCT) through project PPCDT/FIS/60153/2004.

References

[1] Z. Zeng, K. Natesan, Z. Zeng, Fusion Eng. Des. 87–93 (2004) 70.
[2] A. Snis, H. Miettinen, J. Phys. Chem. B 102 (1998) 2555.
[3] E. Henderson, J.E. Bailey, J. Mater. Sci. 28 (1993) 3681.
[4] R.I. Merino, J.A. Pardo, J.I. Pena, G.F. de la Fuente, A. Larrea, V.M. Orera, Phys. Rev. B 56 (1997) 10907.
[5] K. Kukli, M. Ritala, T. Sajavaara, T. Hänninen, M. Leskelä, Thin Solid Films 500 (2006) 322.
[6] M. Boulouz, L. Martin, A. Boulouz, A. Boyer, Mater. Sci. Eng. B, Solid-State Mater. Adv. Technol. 67 (1999) 122.
[7] I.S. Elfimov, S. Yunoki, G. Sawatzky, Phys. Rev. Lett. 89 (2002) 216403.
[8] M.A. Green, D.A. Neumann, Chem. Mater. 12 (2000) 90.
[9] S. Kambe, K. Sato, K. Suezawa, S. Kasuga, S. Ohshima, K. Okeyama, Mater. Chem. Phys. 54 (1998) 190.
[10] P.A. Langjahr, T. Wagner, F.F. Lange, M. Ruhle, J. Cryst. Growth 256 (2003) 162.
[11] H.D. Li, X.N. Zhang, Z. Zhang, Z.X. Mei, X.L. Du, Q.K. Xue, J. Appl. Phys. 102 (2007) 046103.
[12] J.P. Senateur, C. Dubourdieu, F. Weiss, M. Rosina, A. Abrutis, Adv. Mater. Opt. Electron. 10 (2000) 155.
[13] A. Abrutis, J.P. Senateur, F. Weiss, V. Bigelyte, A. Teiserskis, V. Kubilius, V. Galindo, S. Balevicius, J. Cryst. Growth 191 (1998) 79.
[14] A. Abrutis, A. Bartasyte, G. Garcia, A. Teiserskisa, V. Kubiliusa, Z. Saltytea, V. Faucheuxc, A. Figueras, S. Rushworthd, Thin Solid Films 449 (2004) 94.
[15] M. Burriel, G. Garcia, J. Santiso, A. Abrutis, Z. Saltyte, A. Figueras, Chem. Vap. Deposition 11 (2005) 106.
[16] A. Zukova, A. Teiserskis, V. Kazlauskiene, Y.K. Gun'ko, S. van Dijken, J. Magn. Magn. Mater. 316 (2007) e203.
[17] G.S. Hammond, D.C. Nonhebel, C.-H.S. Wu, Inorg. Chem. 2 (1963) 73.
[18] M.A. Saraiva, C.M. Borges, M. Helena Florêncio, J. Mass Spectrom. 41 (2006) 1346.
[19] A.E. Turgambaeva, V.V. Krisyuk, P.A. Stabnikov, I.K. Igumenov, J. Organometallic Chem. 692 (2007) 5001.
[20] Z.L. Wang, A.J. Shapiro, Surf. Sci. 328 (1995) 141.
[21] R. Hull (Ed.), Properties of Crystalline Silicon, Emis Data reviews Series no. 20, The Institution of Electrical Engineers, London, 1999.
[22] P.A. Williams, J.L. Roberts, A.C. Jones, P.R. Chalker, N.L. Tobin, J.F. Bickley, H.O. Davies, L.M. Smith, T.J. Leedham, Chem. Vap. Deposition 8 (2002) 163.
[23] C. Dubourdieu, M. Rosina, H. Roussel, F. Weiss, J.P. Senateur, J.L. Hodeau, Appl. Phys. Lett. 79 (2001) 1246.
[24] R.W. Stark, T. Drobek, W.M. Heckl, Appl. Phys. Lett. 74 (1999) 3296.